ELSEVIER

CrossMark

http://dx.doi.org/10.1016/j.ultrasmedbio.2017.04.012

● *Original Contribution*

CARDIAC SHEAR WAVE ELASTOGRAPHY USING A CLINICAL ULTRASOUND SYSTEM

Mihai Strachinaru,* Johan G. Bosch,[†] Bas M. van Dalen,* Lennart van Gils,*
Antonius F. W. van der Steen,[†‡] Nico de Jong,[†‡] Marcel L. Geleijnse,* and Hendrik J. Vos[†‡]

*Department of Cardiology, Erasmus MC Rotterdam, Rotterdam, The Netherlands; [†]Department of Biomedical Engineering, Erasmus MC Rotterdam, Rotterdam, The Netherlands; and [‡]Department of Acoustical Wavefield Imaging, Delft University of Technology, Delft, The Netherlands

Abstract—The propagation velocity of shear waves relates to tissue stiffness. We prove that a regular clinical cardiac ultrasound system can determine shear wave velocity with a conventional unmodified tissue Doppler imaging (TDI) application. The investigation was performed on five tissue phantoms with different stiffness using a research platform capable of inducing and tracking shear waves and a clinical cardiac system (Philips iE33, achieving frame rates of 400–700 Hz in TDI by tuning the normal system settings). We also tested the technique *in vivo* on a normal individual and on typical pathologies modifying the consistency of the left ventricular wall. The research platform scanner was used as reference. Shear wave velocities measured with TDI on the clinical cardiac system were very close to those measured by the research platform scanner. The mean difference between the clinical and research systems was 0.18 ± 0.22 m/s, and the limits of agreement, from −0.27 to +0.63 m/s. *In vivo*, the velocity of the wave induced by aortic valve closure in the interventricular septum increased in patients with expected increased wall stiffness. (E-mail: m.strachinaru@erasmusmc.nl)   © 2017 The Authors. Published by Elsevier Inc. on behalf of World Federation for Ultrasound in Medicine & Biology. This is an open access article under the CC BY-NC-ND license (http://creativecommons.org/licenses/by-nc-nd/4.0/).

Key Words: Shear waves, Elastography, Stiffness, High-frame-rate tissue Doppler.

INTRODUCTION

Many rapidly occurring mechanical phenomena have been described in the heart, such as electromechanical activation, blood flow noise and shear waves generated in the heart walls by closure of the valves (Cikes et al. 2014; Kanai 2005). The shear waves could potentially be used to estimate non-invasively the stiffness of the myocardium (Brekke et al. 2014; Couade et al. 2011), with huge possible implications for the diagnosis and treatment of multiple pathologies characterized by deterioration of the diastolic properties of the left ventricle. To track these rapidly occurring mechanical waves, high-frame-rate (>200 frames/s) imaging is mandatory. The frame rate in conventional ultrasound imaging is limited by the finite velocity of sound in human tissue (around 1540 m/s) and imaging depth (15 cm in an apical view), as well as the reconstruction of one image frame from many transmit–receive events. This leads to a conventional recording time of about 30 ms per frame, yielding a frame rate of around 30 Hz. Yet, modern clinical scanners achieve frame rates well over 50 Hz in grayscale 2-D imaging by multiline acquisition, in which multiple lines are reconstructed simultaneously from a single transmit–receive event (Tong et al. 2012). Recent approaches to increase the frame rate even further include plane wave imaging or diverging waves, as well as high-level multiline transmit beamforming (Cikes et al. 2014) and selective field-of-view imaging (Brekke et al. 2014; Kanai 2005), which reach frame rates between 500 and 12,000 Hz, depending on the technology and depth of the tissue imaged. Moreover, recent advances in full-channel capture systems indicate that high frame rates can be achieved with relatively high contrast, signal-to-noise ratio (SNR) and sector size (Papadacci et al. 2014), albeit with resolution similar to that of

Address correspondence to: Mihai Strachinaru, Department of Cardiology, Erasmus MC, Room Ba 302, PB 2040, 3000 CA Rotterdam, The Netherlands. E-mail: m.strachinaru@erasmusmc.nl

Conflict of interest disclosure: The authors have no conflicts of interest to disclose.

conventional or multiline acquisition (MLA) beamforming techniques. However, to date, none of these technologies have been implemented in a clinical cardiac ultrasound system (Couade et al. 2011; Konofagou et al. 2011; Lee et al. 2012; Song et al. 2013). On the other hand, current clinical tissue Doppler imaging (TDI) applications use frame rates up to 200 Hz, by multiline acquisition and reduced resolution (Cikes et al. 2014; Sutherland et al. 1999). The use of a clinical scanner to track waves in the human heart has already been described (Pislaru et al. 2014) at frame rates of 350–450 Hz. In this study, we reached higher frame rates in TDI using a clinical cardiac ultrasound system by carefully tuning the imaging parameters, and hypothesized that this fast TDI modality could allow the detection and quantification of shear waves after valve closure. Similar to any other measurement method, both accuracy and precision of the measurement are important in clinical practice. However, such measurement *in vivo* is very difficult because there is no ground truth method for cardiac shear wave tracking, preventing estimation of accuracy, and because every heartbeat is different, preventing estimation of single-shot precision. The core aim of our study therefore was assessment of the accuracy and precision of the clinical TDI method to track shear waves. To obtain a reliable ground truth, we used a phantom setup where the propagation velocity of shear waves is constant and verified by using a high frame rate research scanner.

METHODS

Shear parameters

The *propagation velocity of shear waves* in an isotropic, homogeneous, elastic bulk material is related to the shear modulus μ and density ρ (Shiina et al. 2015) by

$$V_s = \sqrt{(\mu/\rho)} \tag{1}$$

The simplifying conditions (isotropic, homogeneous, elastic, bulk material) will not be met in cardiac tissue, and therefore, we refrained from converting the measured shear wave velocity to shear modulus or Young's modulus E ($E \approx 3 \mu$ in soft biological tissue [Couade et al. 2011]) in the *in vivo* pilot data. However, we presume a monotonic relation between shear wave velocity and tissue stiffness. In the phantom experiment described below, the conditions are well met and this relation is used to convert Young's modulus into an expected shear wave propagation velocity.

Materials

The investigation was carried out on five different tissue ultrasound phantoms (CIRS, Norfolk, VA, USA). The physical properties of these phantoms are summarized in Table 1. Baseline calibration was performed on the multipurpose 40 GSE model, and further testing for different tissue stiffness was performed on the Model 039 phantom set.

We used two ultrasound scanners. The first was a research platform (R) inducing a shear wave through an acoustic radiation force push pulse and tracking it (as reference). It was a Verasonics Vantage system with extended burst option (Verasonics, Kirkland, WA, USA), equipped with a linear array L7-4 probe (Philips, Bothell, WA, USA). Recorded raw channel radiofrequency data and reconstructed ultrasound images were stored for off-line analysis. The second scanner was a normal clinical cardiac ultrasound system (C). This was a Philips iE33 system (Philips Medical, Best, Netherlands) with an S5-1 probe. A two-heartbeat TDI video was recorded and stored in DICOM format for off-line analysis. Philips QLab 9 post-processing software was used for the data analysis.

Setup

In preparation for the measurements, the probes were placed on the upper surface of the phantom, using clinical ultrasound gel as a contact medium. The probes were carefully aligned with their 2-D sectors in-line and thus oriented perpendicular to the direction of propagation of the shear wave. The leads of both an external cardiotachometer (CWE CT-1000) and the clinical scanner were attached to one of the researchers (M.S.) to

Table 1. Tissue phantom properties

Phatom properties	Model 40 GSE Calibration phantom	Model 039 Phantom 1	Phantom 2	Phantom 3	Phantom 4
Expected shear wave velocity	2.80 m/s	1.01 m/s	1.57 m/s	2.43 m/s	3.56 m/s
Young's modulus E	25 kPa	2.7 kPa	11 kPa	20 kPa	48 kPa
Density			1030 kg/m³		
Poisson ratio			0.5		
Attenuation			0.5 dB/cm/MHz		
Velocity of sound			1540 m/s		

synchronize the R and C scanners through the electrocardiograph signal. The cardiotachometer produced a trigger signal at the QRS peak, which initiated the R system to generate an acoustic radiation force push pulse at a depth of 32 mm. In alternating paired recordings, the resulting shear wave was detected either with the R scanner for reference or with the C scanner for its characterization. To avoid cross talk between the tracking pulses of the two scanners, the imaging of the shear wave with the R scanner was performed with C in freeze mode. Reciprocally, when investigating waves with the C system, the R scanner was used to induce the acoustic push only.

The acquisitions were performed on separate days, with intermittent probe repositioning, varied locations of the push pulse and variation of the acquisition settings. To obtain the maximum frame rate with the C system, a depth of 6 cm was investigated. The XRes image enhancement modality was turned off, and the 2-D line density was set to minimum and the TDI frame rate to maximum. Smoothing and persistence settings were also minimized. The ultrasound frequency was set to 3.4 MHz, and the velocity range to ± 1.5 cm/s. The frame rate range achieved was between 420 and 645 Hz, depending mainly on the opening of the TDI field of view. At this depth, a 4-cm maximal opening (40°) of the TDI sector can provide 470 Hz; a 3-cm opening (30°), 570 Hz; and a 2-cm opening (20°), 645 Hz. The maximal frame rate is thus highly dependent on sector opening. Yet, because shear wave tracking requires both a high temporal resolution and a wide field of view, there may be an optimal setting at which the combination of frame rate and sector width produces the most accurate and precise results. This optimal setting was investigated by analyzing three frame rates ranges (400–500, 500–600 and 600–700 Hz).

In vivo *data*

A normal healthy volunteer and two patients were tested using the same setup as for the clinical scanner. This research was approved by the local medical ethics committee, and informed consent was obtained from all patients. At a depth of 9 cm, we obtained more than 500 Hz for a window opening of 3 cm (20°) (suitable for parasternal application).

Data processing

Research scanner setup. The characteristics of the acoustic radiation force push pulse and the tracking pulses are outlined in Table 2.

Data processing for the research scanner. The analytical signal $S(x, z, i)$ in frame i for every pixel at (x, z) was generated by the internal Verasonics image reconstruction algorithm. In the what follows, the (x, z)

coordinates within the parentheses are omitted for simplicity. Local tissue velocity $v(i)$ was obtained with a phase estimator for every pixel based on the cross-correlation of the analytic signal with temporal lag one (Brekke et al. 2014):

$$R_1(i) = S(i) \cdot S * (i-1) \qquad (2)$$

$$v(i) = v_N \cdot \angle R_1(i)/\pi \qquad (3)$$

$$v_N = c \cdot F/(4 \cdot f_c) \qquad (4)$$

Here, R_1 is the cross-correlation value per pixel for a time offset of 1 frame, the asterisk denotes the complex conjugate, $\angle$ denotes the angle (rad), v_N is the Nyquist velocity, f_c is the center frequency of the pulse, c is the velocity of sound in the medium and F is the frame rate. The value of the Nyquist velocity was 0.35 m/s, which was high enough to avoid any aliasing effect in the local tissue velocity measurements.

Similar to Brekke et al. (2014), we applied a spatial smoothing filter to the cross-correlation frames R_1 (eqn [2]) before calculating the phase (eqn [3]) to remove the influence of speckle. This smoothing consisted of a moving average filter 1.5 mm in size in both the axial and lateral directions, which is on the same order as the speckle size in the research system. Because the wavelength of the mechanical waves was around 10 mm, the chosen kernel size did not reduce the signal levels significantly.

The resulting local particle velocity $v(i)$ is a data set containing subsequent TDI frames at a frame rate equal to the original frame rate. Along a horizontal virtual M-mode line located at the depth of the push pulse (32 mm), the forward propagating wave was extracted and gathered in a 2-D panel. This panel thus illustrates the wavelet propagating as a function of time and distance along the M-mode line (Fig. 1).

The slope $\Delta x/\Delta t$ with which this wave propagates is the propagation velocity that acts as the ground truth to the wave propagation measured with the clinical scanner. Yet, in the data processing of the clinical scanner, we

Table 2. Research scanner setup and parameters

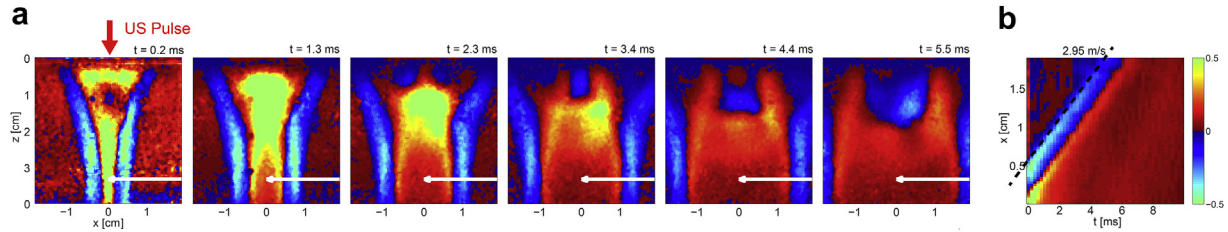|	
Acoustic radiation force pulse	
Center frequency	4 MHz
Duration	1.4 ms (5600 cycles)
F Number	1.5
Driving voltage	60 V
Tracking	
Center frequency	5.2 MHz
Duration	0.4 μs (2 cycles)
Transmit type	Three angled plane waves
Driving voltage	60 V
Frame rate	4762 Hz

Fig. 1. Shear wave propagation as detected by the research system. (a) High-frame-rate tissue Doppler images of travelling shear waves. The shear waves are displacing away from the external acoustic radiation force push focal zone, in a few selected successive frames; time is noted, with t = 0 ms at the push. The *white arrow* represents the virtual M-mode line. (b) Virtual M-mode along the line in (a). The slope of the wave front is tracked with a Radon transform in a region of interest with the research system, giving a velocity estimate of 2.95 m/s in this recording.

tracked the wave *front*, which is most clearly visible for the observer. In the data processing of the research scanner, we wanted to automate the tracking, for which the Radon transform produces an accurate outcome (Rouze et al. 2010; Urban and Greenleaf 2012). The Radon transform tracks the wave *peak* path. To match the wave *front* tracking in the clinical scanner with the wave *peak* tracking in the research scanner, we first took a time derivative of the local particle velocity in the research scanner. This effectively yielded a map containing the local particle *acceleration*, with the rationale that the wave front correlates to the first trace of highest magnitude in this acceleration map. Next, we extracted the slope of the trace using a Radon transform in the region of interest (Rouze et al. 2010; Urban and Greenleaf 2012; Vos et al. 2015).

Data processing for the clinical scanner. The DICOM TDI loops (DICOM pixel array of 768 rows and 1024 columns, with a pixel spacing of 0.088/0.088 mm) were processed using QLab 9. A virtual M-mode line was horizontally traced across the TDI sector at the depth of the focal point of the push pulse, which was applied to the left, immediately outside the sector (Fig. 2a). Its length and direction were predefined by the user. For consistency, we chose the that the M-mode line always point toward the shear wave source, perpendicular to the wave front. The velocity propagation of the wave front was estimated with

$$V_s = D/T \qquad (5)$$

where D is the (user-defined) length of the M-mode line, and *T* is the time the wave travels along the M-mode line.

The software provides a virtual M-mode map (Fig. 2b), allowing us to manually trace the slope of the propagating wave. This map does not display a time axis in QLab. Yet, the propagation time *T* can be obtained through a work-around. By manually clicking on the base and top of the slope of the wave, the program returned the corresponding active points on the time–velocity curve

that is automatically computed by the software (Fig. 2c). The time interval *T* between these points is then displayed automatically (Fig. 2d). From this time, and pre-defined M-mode length, the velocity is calculated (Fig. 2 and eqn [5]).

Statistical analysis

Baseline testing and calibration were performed on the 40 GSE phantom. Thirty independent paired measurements were performed on this tissue phantom. The resulting velocities were represented as the mean ± standard deviation (SD). Differences between mean values were estimated with the paired-sample *t*-test. If not normally
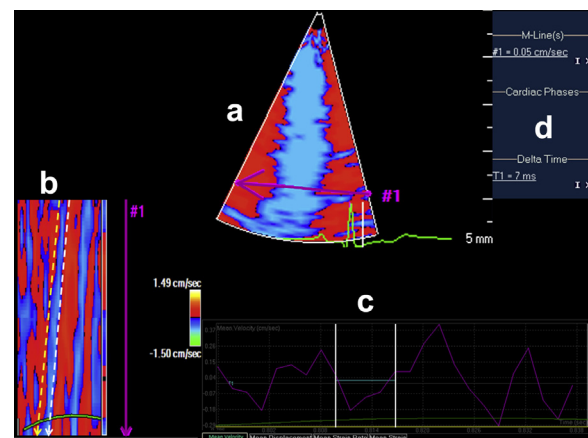

Fig. 2. Detailed view (modified to indicate the main elements) of the data obtained in the tissue phantom, using off-line processing in Philips QLab. The electrocardiogram signal belongs to one of the researchers (M.S.) and was only used to synchronize the two ultrasound systems. In the spatiotemporal color map, we highlighted the moving wave front with *dotted arrows* for clarity. (a) Virtual M-mode line (#1) traced across the TDI sector. (b) Virtual M-mode map of a shear wave illustrating the wave front (*leftmost dotted arrow*) and the first velocity zero crossing (*rightmost dotted arrow*). (c) Mean velocity curve (averaged over the M-mode line). The time interval in which the wave occurs is delineated by the *solid white lines*. (d) Results panel, revealing the time interval.

Table 3. Tissue phantoms shear wave velocities according to the clinical (C) and research (R) scanner

Phantom	Model 40 GSE	Model 039 phantom 1	Model 039 phantom 2	Model 039 phantom 3	Model 039 phantom 4
Expected shear wave velocity	2.80 m/s	1.01 m/s	1.57 m/s	2.43 m/s	3.56 m/s
Clinical scanner velocity	2.85 ± 0.21 m/s (N = 7)	1.06 ± 0.05 m/s (N = 7)	1.59 ± 0.08 m/s (N = 6)	2.76 ± 0.17 m/s (N = 5)	3.87 ± 0.21 m/s (N = 7)
Research scanner velocity	2.87 ± 0.07 m/s	0.87 ± 0.01 m/s	1.51 ± 0.02 m/s	2.34 ± 0.01 m/s	3.56 ± 0.07 m/s

distributed, the data sets were also compared using the Wilcoxon signed-rank test. The distribution was represented by boxplots. Testing for other stiffness values (other shear wave velocities) was performed with an additional five to seven paired measurements for each of the five phantoms. Variability was calculated as 1.96 SD of the mean arithmetical difference according to Bland and Altman. *Accuracy* was defined as the proximity of the mean value to the reference value; *precision* as the closeness of the agreement between results (represented by the standard deviation). For the calibration study, standard error was also calculated to support the assessment of accuracy. Inter- and intra-observer variability for the clinical scanner was assessed on 10 randomly chosen acquisitions. Intra-observer test–retest variability was evaluated on the initial measurements performed by M.S. with a new measurement set one 1 later, blinded to the first result. Inter-observer variability was estimated between the results of M.S. and the results obtained by a first-time user, without any prior knowledge of the experiment or the software application (L.G.). SPSS software (Version 21, IBM, Armonk, NY, USA) was used for all analyses, with a p value < 0.05 considered to indicate significance.

RESULTS

Both scanners detected the waves propagating away from the push region over a time span that varied with the phantom's stiffness (Figs. 1 and 2; Supplementary Video S1, online only, available at http://dx.doi.org/10.1016/j.ultrasmedbio.2017.04.012). We measured the propagation velocity of the wave front.

Research scanner

The automated detection algorithm was used to track the wave front, resulting in a velocity of 2.87 ± 0.07 m/s in the calibration phantom and different velocities in the Model 039 phantoms (Table 3).

Clinical scanner

Frame rate calibration. The propagation velocities of the wave front of the shear wave in the calibration phantom at different frame rate ranges of the C scanner are summarized in Table 4. The velocity ranged between 2.77 ± 0.14 and 2.83 ± 0.18 m/s, depending on the frame rate (Fig. 3). The velocities recorded at frame rates of 500–600 and 600–700 Hz were statistically similar to the R scanner results (lowest mean difference of -0.04 ± 0.20 m/s, Wilcoxon $Z = -0.99$, $p = 0.318$ for the frame rate range 500 to 600 Hz). The limits of agreement were smaller than ± 0.45 m/s (Table 4).

Table 4. Difference between velocities calculated by the clinical and research scanners, according to the frame rate range of the clinical system, for calibration

| Frame rate range | Paired-sample *t*-test | | | | Bland–Altman | | Wilcoxon signed-rank test | | | |
	C Scanner speed, m/s (mean ± SD)	SEM	95% CI	*p* value	Difference between C and R scanners* (mean ± SD)	Limits of agreement (±1.96 SD)	*t*-statistic	Z	*p* value	*r* (effect size)
400–500 Hz	2.77 ± 0.14	0.028	0.04 to 0.16	0.002	−0.09 ± 0.16	−0.39 to 0.22	8	−2.75	0.006	−0.50
500–600 Hz	2.83 ± 0.18	0.037	−0.04 to 0.12	**0.298**†	−0.04 ± 0.20	−0.43 to 0.35	14	−0.99	**0.318**	−0.18
600–700 Hz	2.80 ± 0.18	0.037	−0.01 to 0.14	**0.075**	−0.06 ± 0.20	−0.30 to 0.45	13	−1.80	**0.072**	−0.33

C = clinical; CI = confidence interval; R = research; SD = standard deviation; SEM = standard error of the mean.
* R scanner speed was 2.87 ± 0.07 m/s.
† Non-significant *p* values are highlighted in boldface.

Velocity measurements using the calibrated settings. A new measurement set was performed on all five phantoms, using the best-fitted settings from the calibration (frame rate of 513 Hz). The results are summarized in Table 3. Velocities measured with the two scanners were similar and close to the reference values.

Intra- and inter-observer variability. For intra-observer test–retest variability (No. = 10 readings), the first reading displayed a velocity of 2.73 ± 0.13 m/s. At the second reading, the mean value was 2.81 ± 0.08 m/s ($p = 0.10$). The mean difference was −0.07 ± 0.13 m/s. The limits of agreement were −0.33 to +0.18 m/s.

For inter-observer variability, the mean value of velocity obtained by the second observer (No = 10 readings) was 2.92 ± 0.25 m/s ($p = 0.08$). The mean difference between observers was −0.19 ± 0.29 m/s. The limits of agreement were −0.76 to +0.38 m/s.

Accuracy. Taking the measurements of the R scanner as reference, the difference in the measurements obtained by the clinical scanner was assessed on the last set of five to seven paired measurements performed with each of the five phantoms. The correlation between the two scanners (Fig. 4a) was excellent ($R^2 = 0.952$, $p < 0.0001$). The mean difference between the clinical
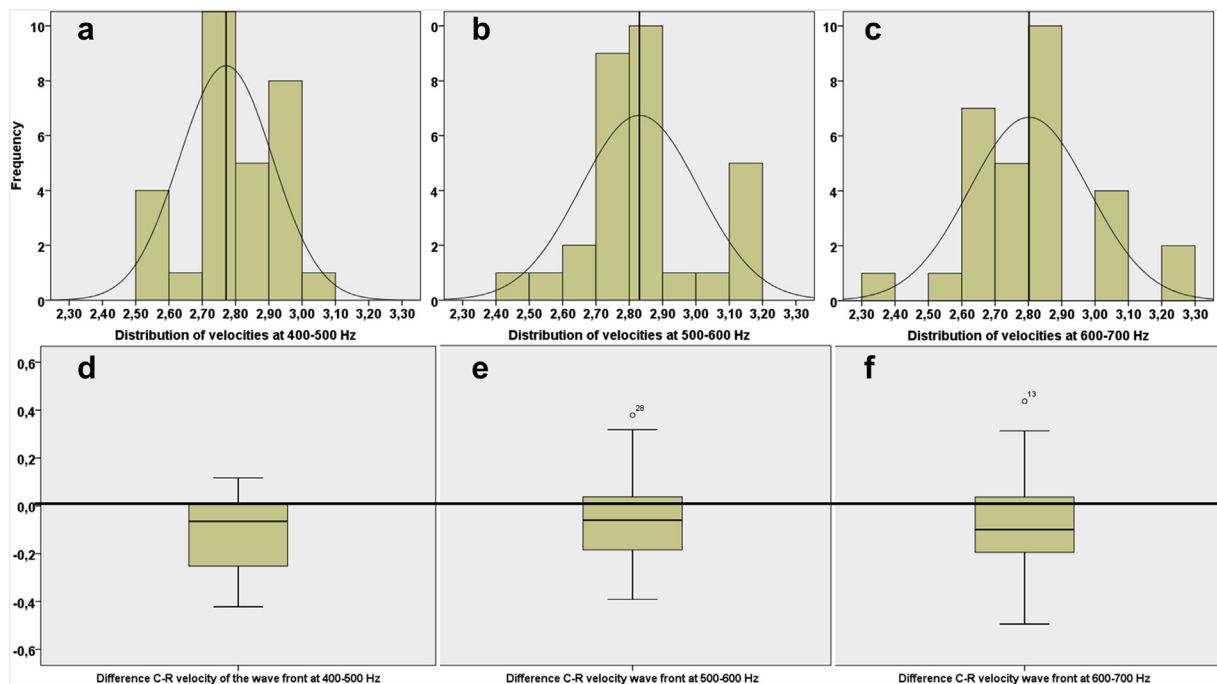

Fig. 3. Calibration study. The distribution of velocities measured at different frame rate ranges (a–c) and the difference in measured velocity between the clinical and research systems (d–f) are compared in boxplots, illustrating the bias and distribution of the differences. Frame rate ranges = (a,d) 400 to 500 Hz; (b,e) 500 to 600 Hz; and (c,f) 600 to 700 Hz. The mean velocity is marked by a *vertical line* in (a)–(c). The *horizontal line* in the lower panels marks the zero point (perfect agreement).
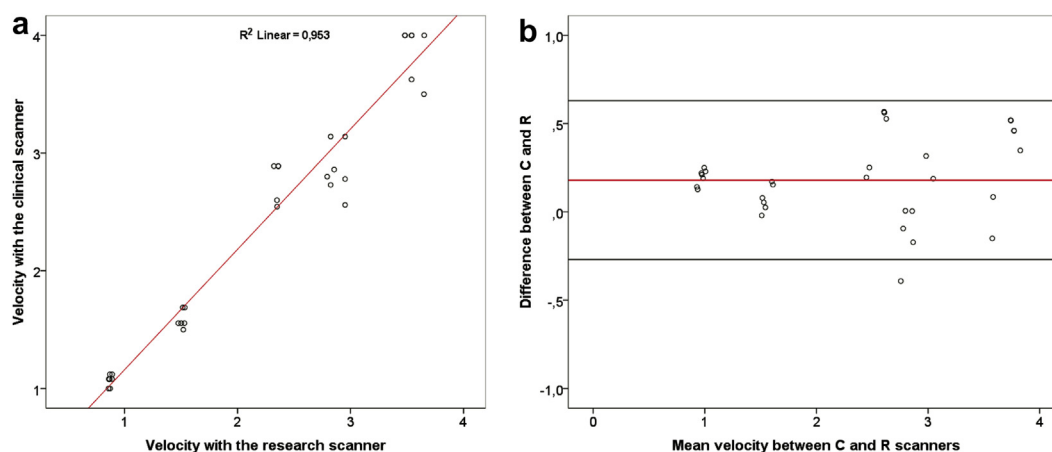
Fig. 4. Accuracy study. (a) Correlation of the velocities measured with the two systems. (b) Bland–Altman analysis of the agreement between the two scanners. C = clinical scanner; R = research scanner.

and the research systems was 0.18 ± 0.22 m/s, and the limits of agreement, from -0.27 to $+0.63$ m/s (Fig. 4b).

In vivo *detection of shear waves in patients*

A 28-y-old healthy man underwent a cardiac ultrasound examination with simultaneous recording of the electrocardiogram (ECG) and phonocardiogram. High-frame-rate TDI (510 Hz at 8-cm depth, velocity scale: 3.5 cm/s) signals were acquired from the parasternal window, from the proximal part of the interventricular septum. The velocity of the shear wave

traveling into the septal wall after aortic valve closure was 3.0 m/s for an M-mode line traced at midwall level (Fig. 5a).

In a 43-y-old female patient with a dilated ischemic cardiomyopathy, high-frame-rate TDI (513 Hz at 8-cm depth, velocity scale: 2.5 cm/s) revealed a velocity of 4.4 m/s (Fig. 5b; Supplementary Video S2, online only, available at http://dx.doi.org/10.1016/j.ultrasmedbio.2017.04.012). The shear wave is clearly separated from the myocardial displacement occurring in early isovolumetric relaxation.
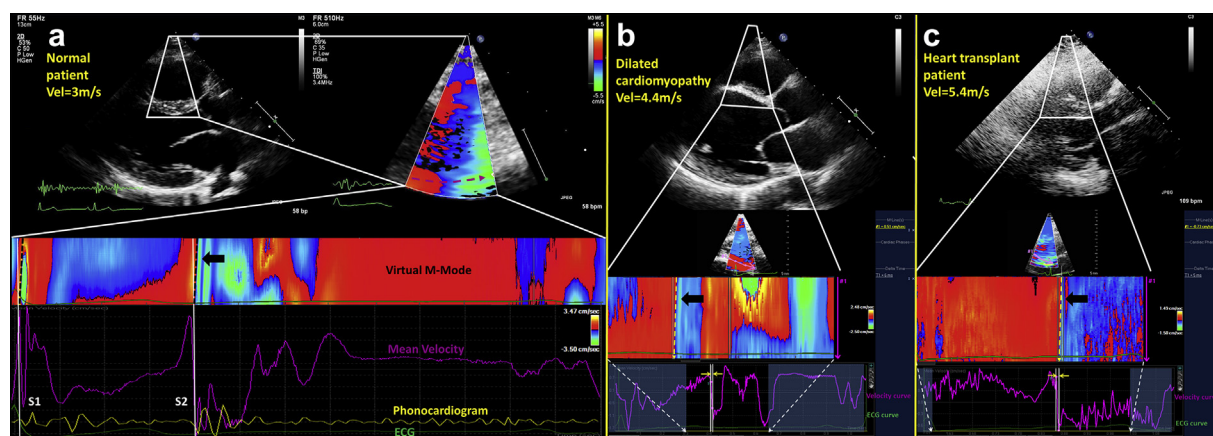

Fig. 5. Clinical application of the high-frame-rate tissue Doppler technique. (a) Normal male subject. The wave front is synchronous with the onset of the second heart sound (S2) on the phonocardiogram (PCG); the velocity is computed at 3.0 m/s; the shear wave after mitral valve closure is also visible synchronous with the first heart sound (S1). Top panels: Classic echocardiographic image and focused TDI window over the interventricular septum. Lower panels: one full cardiac cycle was reconstructed off-line; the slope of the aortic shear wave (*black arrow*), extracted from the virtual M-mode, is marked with a *dashed line*. (b) Dilated cardiomyopathy. The velocity of the wave front reaches 4.4 m/s. (c) Heart transplant patient; the velocity of the shear wave is even higher, computed at 5.4 m/s. At a velocity scale of 1.5 cm/s, a velocity shift (zero crossing) is seen separating the shear wave (*black arrow*). Time intervals are extracted from the velocity/time curves and underlined by *vertical white lines*. The M-mode map displays only a fraction of the cardiac cycle around the closure of the aortic valve (depending on the relation frame rate *vs.* heart rate). This corresponds to the clear window in the velocity/time/electrocardiogram panels and is indicated with *white dashed arrows*. C = clinical scanner; R = research scanner.

A 48-y-old male patient who had received a heart transplant 9 mo before, with signs of rejection, underwent a routine ultrasound examination. Although the image quality was poor, the left ventricular walls could still be visualized. A high-frame-rate TDI acquisition (541 Hz, 9-cm depth, velocity scale: 1.5 cm/s) in the parasternal view was added that revealed a fast wave traveling into the septum after the aortic valve closure, similar to the other cases, but at a velocity of 5.4 m/s (Fig. 5c).

DISCUSSION

The main findings of this study were as follows: (i) The visualization of shear waves induced by acoustic radiation force into a tissue phantom is possible with a clinical TDI application, at a surprisingly high frame rate (400–645 Hz). (ii) The waves can be tracked and their velocity quantified in this *in vitro* setting, with sufficient precision and accuracy at a frame rate range greater than 500 Hz. (iii) *In vivo* tracking is feasible in patients, and the results seem to confirm that the velocity of the waves is increasing where increased wall stiffness is expected based on pathology.

In several studies, the detection of rapidly occurring phenomena in the heart has been described (Brekke et al. 2014; Cikes et al. 2014; Kanai 2005; Kanai et al. 2000; Pernot et al. 2011), using experimental systems or modified software. In our study a normal modern clinical scanner achieved surprisingly high TDI frame rates, between 400 and 700 Hz at depths less than 10 cm, by turning off image enhancement modalities and by carefully tuning the relationship between the depth of the image, the 2-D line density and aperture and the TDI field of view. We hypothesized that the time resolution of 2 ms (500 Hz frame rate) could allow the detection and quantification of the very fast phenomena that are naturally occurring in the heart, such as shear-like waves caused by t closure of the valves. The present study indicates that shear waves in a tissue phantom are accurately detected by the TDI clinical application. As the reference wave velocity could be validated by the research scanner, both the accuracy and precision of the method were investigated.

The precision of the measurement is restricted by the field of view (represented by M-mode length D) and frame rate (F) in the clinical scanner. With respect to eqn (5), the standard deviation in the propagation speed δV_s can be caused by variance in both D and T. Standard deviation in D is caused by limited lateral resolution R (Elegbe and McAleavey 2013) in the sector of the phased array probe (despite the fixed length of the virtual M-mode line). Variance in T is caused by rounding off to integer frame intervals. Application of the generic equations of statistically independent variables to eqn (5)

gives the approximate equation (see Appendix A for details)

$$\delta V_s = V_s/D\sqrt{\{(R/2)^2 + 1/6 \cdot (V_s/F)^2\}} \qquad (6)$$

For example, at a width of 3.5 cm for the TDI window, a frame rate of 500 Hz and a typical speckle size of 5 mm, a wave with 2.8 m/s propagation velocity has an expected standard deviation of 10%, which is similar to the value actually observed (6%). For a wave traveling at 5 m/s, the expected value increases to 14% because of the relatively increased influence of frame rate (see also Table 3). The standard deviation can be improved only by taking the average over multiple recordings. On the contrary, the research system has both a higher temporal and spatial resolution thanks to a larger linear probe, higher imaging frequency and full channel acquisition. This allows for very precise single measurements.

In the calibration measurements, the average propagation velocities yielded by the clinical scanner were statistically similar to the research velocities in the frame rate ranges 500–600 Hz (2.83 ± 0.18 m/s, $p = 0.298$) and 600–700 Hz (2.80 ± 0.18 m/s, $p = 0.075$). In conventional echocardiographic measurement (Chukwu et al. 2008; Lang et al. 2015), mean percentage errors are reported to be around 10%–20%, similar to the errors in our findings. The precision was increased in the calibration study by averaging 30 measurements, resulting in a standard error of around 0.04 m/s (1% relative error). These settings were used for the accuracy study, which revealed tight limits of agreement, comparable to the measurement variability. The inter-observer variability was of the same magnitude as the difference between individual measures. On the basis of these values, the accuracy and precision can be considered acceptable for research purposes. The clinical relevance of this variability remains to be established, being dependent on the physiologic or pathologic range of velocities.

Clinical application

In past years we developed a high-frame-rate ultrasound imaging modality that determined the propagation velocity of Lamb waves (which are shear wave-like) in the septal wall (Vos et al. 2017), which are natural and caused by aortic and mitral valve closure. The recorded velocities are in close agreement with those obtained with an alternative method that uses externally induced shear waves, which, however, is either insensitive (Song et al. 2013) or invasive (Hollender et al. 2012). Other teams have been working on clinical TDI with modified software to achieve the very high frame rate needed to image these phenomena (Brekke et al. 2014). Our *in vivo* data indicate that shear waves can be measured with a

clinical system in cardiac mode, which could, in one step, make the translation from laboratory research to clinical research or even everyday clinical practice, without major investments in new equipment or software.

Because Doppler is most sensitive for axial motion, it has the highest sensitivity in detection of shear waves propagating laterally in the field of view, at a TDI velocity scale adapted to match the particle velocity. Please note that although the angle between the propagation direction and the ultrasound beam may influence the apparent amplitude of the shear wave, it has no influence on the apparent propagation velocity, the latter being the property of interest in the present study. Translating these properties into clinical echocardiography, a TDI system would be most sensitive for shear waves traveling through the interventricular septal wall in a *parasternal* view, rather than in an *apical* view. We tested the technique (using the same clinical scanner, probe and TDI settings used to obtain the experimental results) on a healthy individual and on individuals with several typical pathologies modifying the consistency of the left ventricular wall. The velocity scale allowing for clear visualization of the shear wave matches the particle displacement velocity observed in previous studies (1.5–3 cm/s) (Brekke et al. 2014; Vos et al. 2015). The velocity of the wave induced in the interventricular septum seems to increase in the cases in which the stiffness of the wall is expected to increase, compared with the healthy individual. Although no definitive conclusion can be drawn, these limited data indicate that the detection and quantification of these naturally occurring shear-like waves are feasible in patients, and could represent a direct measurement of wall stiffness, with potential implications in multiple pathologies characterized by a deterioration of the left ventricular function.

In the present *in vivo* study, we focused on aortic valve closure. However, the waves after mitral valve closure were also detectable in our study patients, as observed on the M-mode map in Figure 5a and Video S2 (leftmost at the beginning of the video). Thus, the detection method can record the stiffness during two moments in the cardiac cycle: when the muscle is dilated and when it is compact. Specific relations between the two points (ratio, difference) may have clinical relevance other than their individual values because of cancellation of possible confounding factors such as preload, afterload and wall thickness, although such relevance needs to be thoroughly tested in a larger study population. During the short isovolumetric periods in which the waves propagate, there is only minor motion of the myocardial walls, making shear wave quantification presumably easier and more reliable. On the other hand, the intrinsic myocardial stiffness may vary over the short period in which the waves propagate (on the order of 10–20 ms), thus chang-

ing the instantaneous shear wave speed. Although Kanai (2005) reported a time dependency of the wave propagation velocity after aortic valve closure, we have not observed such a phenomenon in our data. Yet, to further elucidate this phenomenon, the dynamic components of stiffness may be studied, for example, in a more experimental setup involving accurately timed acoustic radiation force shear wave elastography.

Strain, strain rate and data derived from TDI velocities are recent applications that assess myocardial deformation and, indirectly, elasticity. A down side of these methods is a great dependence on hydrodynamic parameters (preload, afterload), as strain is a ratio of pressure and myocardial stiffness. Although a dependency may also exist in the shear wave method, it is expected to be weaker because hydrodynamic pressure is not found in the principal relation between shear wave propagation velocity and stiffness. A comparison with the high-frame-rate TDI-derived shear wave velocity may be further studied based on data recorded with the same clinical scanner.

The myocardial wall exhibits a complex fiber structure, so shear wave propagation might be inhomogeneous across the width of the septum. For simplicity, in our *in vivo* data, we chosen the midwall position, having presumably the highest consistency in placement. Further clinical studies are warranted to detect and characterize this phenomenon.

The propagation velocity in our healthy subject was lower than that for a group of 10 human patients studied by Brekke et al. (2014) (5.41 $\pm$ 1.28 m/s) specifically and more generally found in human and animal studies (Hollender et al. 2012). We speculate that this difference originates from the different probe positioning: parasternal in our study and apical in Brekke et al. (2014) and Kanai et al. (2000).

The longitudinal myocardial stretch during late diastole, as described by Pislaru et al. (2014), was also visible in our human patients. The expected velocity of these phenomena is between 1 and 2 m/s, which can be easier to track with lower frame rates than the faster waves after aortic valve closure.

Unfortunately, the exact TDI beamforming technique and settings are not disclosed on the clinical system, although it is known that the Philips iE33 implements an MLA technique. Yet, we could make a general estimation based on the work by Tong et al. (2012), who compared various fundamental-frequency MLA beamforming techniques. The speckle size in our color TDI videos was 4–5 mm in the lateral direction. Tong et al. calculated lateral beamwidths on the order of 2–3 mm up to a depth of 50 mm, and 3–5 mm for imaging depths >50 mm. Although significant differences exist between the specific implementations of MLA, the differences are relatively small, and the values are very

similar to our measurements. This implies a reasonably good resolution in our current TDI measurements. As discussed by Papadacci et al. (2014), more recent full-channel capture systems, which enable an extremely high degree of MLA and compounding, do not improve on resolution, but they will simultaneously improve on contrast, SNR, imaging sector size and frame rate. Of these aspects, SNR proved to be sufficient in our measurements, but a larger image sector and slightly higher frame rate (on the order of 1000 frames/second) would reduce the variance in the measurements, according to eqn (6). The effect of a higher image contrast has yet to be studied in a more realistic phantom with higher tissue contrast. Therefore, although measurement precision may be improved with recent full-channel capture systems, the performance of the currently used clinical scanner is reasonably good.

Study limitations and future directions

One limitation of the study may be the limited velocity range of the phantom set (1–4 m/s), although the results indicate neither signs nor trends of bias for these velocities. Further confirmation of the strength of the method should come from clinical studies with a broad pathology spectrum. The present work indicates that shear waves can be measured with good consistency with a regular clinical scanner, thus opening the way to more *in vitro* and *in vivo* studies.

As mentioned above, a TDI frame rate of 500 Hz could be insufficient when it comes to higher velocities, because such waves would quickly travel through the limited field of view. We hope that advancement in technology, resulting in the availability of higher frame rates, and/or the changes in data processing would allow the use of wider fields of view.

Manual tracking as allowed by the manufacturer-designed software is time consuming and vulnerable to errors. Therefore, future research should focus on a robust method of automated velocity tracking from the DICOM frames. A possible candidate for such robust analysis is the Radon transform as illustrated in this study for the research scanner data.

CONCLUSIONS

A regular clinical cardiac TDI application can visualize and quantify shear waves induced by acoustic radiation force in a tissue phantom at sufficiently high frame rates (on the order of 500 Hz). *In vivo* tracking is feasible in patients, and the results seem to confirm that the velocity of the waves is increasing where increased wall stiffness is expected based on pathology.

SUPPLEMENTARY DATA

Supplementary data related to this article can be found online at http://dx.doi.org/10.1016/j.ultrasmedbio.2017.04.012.

REFERENCES

Brekke B, Nilsen LC, Lund J, Torp H, Bjastad T, Amundsen BH, Stoylen A, Aase SA. Ultra-high frame rate tissue Doppler imaging. Ultrasound Med Biol 2014;40:222–231.

Chukwu EO, Barasch E, Mihalatos DG, Katz A, Lachmann J, Han J, Reichek N, Gopal AS. Relative importance of errors in left ventricular quantitation by two-dimensional echocardiography: Insights from three-dimensional echocardiography and cardiac magnetic resonance imaging. J Am Soc Echocardiogr 2008;21:990–997.

Cikes M, Tong L, Sutherland GR, D'hooge J. Ultrafast cardiac ultrasound imaging: technical principles, applications, and clinical benefits. JACC Cardiovasc Imaging 2014;7:812–823.

Couade M, Pernot M, Messas E, Ba M, Hagege A, Fink M, Tanter M. In vivo quantitative mapping of myocardium stiffening and transmural anisotropy during the cardiac cycle. IEEE Trans Med Imaging 2011;30:295–305.

Elegbe EC, McAleavey SA. Single tracking location methods suppress speckle noise in shear wave velocity estimation. Ultrason Imaging 2013;35:109–125.

Hollender PJ, Wolf PD, Goswami R, Trahey GE. Intracardiac echocardiography measurement of dynamic myocardial stiffness with shear wave velocimetry. Ultrasound Med Biol 2012;38:1271–1283.

Kanai H. Propagation of spontaneously actuated pulsive vibration in human heart wall and in vivo viscoelasticity estimation. IEEE Trans Ultrason Ferroelectr Freq Control 2005;52:1931–1942.

Kanai H, Yonechi S, Susukida I, Koiwa Y, Kamada H, Tanaka M. Onset of pulsatile waves in the heart walls at end-systole. Ultrasonics 2000;38:405–411.

Konofagou E, Lee WN, Luo J, Provost J, Vappou J. Physiologic cardiovascular strain and intrinsic wave imaging. Annu Rev Biomed Eng 2011;13:477–505.

Lang RM, Badano LP, Mor-Avi V, Afilalo J, Armstrong A, Ernande L, Flachskampf FA, Foster E, Goldstein SA, Kuznetsova T, Lancellotti P, Muraru D, Picard MH, Rietzschel ER, Rudski L, Spencer KT, Tsang W, Voigt JU. Recommendations for cardiac chamber quantification by echocardiography in adults: An update from the American Society of Echocardiography and the European Association of Cardiovascular Imaging. J Am Soc Echocardiogr 2015;28:1–39.e14.

Lee W, Pernot M, Couade M, Messas E, Bruneval P, Bel A, Hagège AA, Fink M, Tanter M. Mapping myocardial fiber orientation using echocardiography-based shear wave imaging. IEEE Trans Med Imaging 2012;31:554–562.

Papadacci C, Pernot M, Couade M, Fink M, Tanter M. High-contrast ultrafast imaging of the heart. IEEE Trans Ultrason Ferroelectr Freq Control 2014;61:288–301.

Pernot M, Couade M, Mateo P, Crozatier B, Fischmeister R, Tanter M. Real-time assessment of myocardial contractility using shear wave imaging. J Am Coll Cardiol 2011;58:65–72.

Pislaru C, Pellikka PA, Pislaru SV. Wave propagation of myocardial stretch: correlation with myocardial stiffness. Basic Res Cardiol 2014;109:438.

Rouze NC, Wang MH, Palmeri ML, Nightingale KR. Robust estimation of time-of-flight shear wave speed using a radon sum transformation. IEEE Trans Ultrason Ferroelectr Freq Control 2010;57:2662–2670.

Shiina T, Nightingale KR, Palmeri ML, Hall TJ, Bamber JC, Barr RG, Castera L, Choi BI, Chou YH, Cosgrove D, Dietrich CF, Ding H, Amy D, Farrokh A, Ferraioli G, Filice C, Friedrich-Rust M, Nakashima K, Schafer F, Sporea I, Suzuki S, Wilson S, Kudo M. WFUMB guidelines and recommendations for clinical use of

ultrasound elastography: Part 1. Basic principles and terminology. Ultrasound Med Biol 2015;41:1126–1147.

Song P, Zhao H, Urban M, Manduca A, Pislaru S, Kinnick R, Pislaru C, Greenleaf J, Chen S. Improved shear wave motion detection using pulse-inversion harmonic imaging with a phased array transducer. IEEE Trans Med Imaging 2013;32:2299–2310.

Sutherland GR, Bijnens B, McDicken WN. Tissue Doppler Echocardiography: Historical perspective and technological considerations. Echocardiography 1999;16:445–453.

Tong L, Gao H, Choi HF, D'hooge J. Comparison of conventional parallel beamforming with plane wave and diverging wave imaging for cardiac applications: a simulation study. IEEE Trans Ultrason Ferroelectr Freq Control 2012;59:1654–1663.

Urban MW, Greenleaf JF. Use of the radon transform for estimation of shear wave speed. J Acoust Soc Am 2012;132:1982.

Vos HJ, van Dalen BM, Bosch JG, van der Steen AFW, de Jong N. Myocardial passive shear wave detection, Proceedings of the IEEE International Ultrasonics Symposium. Taipei, Taiwan: IEEE; 2015. p. 1–4.

Vos HJ, van Dalen BM, Heinonen I, Bosch JG, Sorop O, Duncker DJ, van der Steen AF, de Jong N. Cardiac shear wave velocity detection in the porcine heart. Ultrasound Med Biol 2017;43:753–764.